Supplementary Materials

Fluorine-expedited nitridation of layered perovskite Sr_2TiO_4 for visible-light-driven photocatalytic overall water splitting

Jinxing Yu[1#], Jie Huang[2,3#], Ronghua Li[4], Yanbo Li[4], Gang Liu[2,3]*, Xiaoxiang Xu[1]*

[1]Shanghai Key Lab of Chemical Assessment and Sustainability, School of Chemical Science and Engineering, Tongji University, Shanghai, 200092, China

[2]Shenyang National laboratory for Materials Science, Institute of Metal Research, Chinese Academy of Sciences, 72 Wenhua Road, Shenyang 110016, China,

[3]School of Materials Science and Engineering, University of Science and Technology of China, 72 Wenhua Road, Shenyang 110016, China

[4]Institute of Fundamental and Frontier Sciences, University of Electronic Science and Technology of China, Chengdu, China

[#] These authors contributed equally to this work.

* Correspondence: gangliu@imr.ac.cn, xxxu@tongji.edu.cn

Supplementary Tables

Supplementary Table 1. Space group, refined unit cell parameters and BET surface area of as-prepared samples, standard deviation is included in the parenthesis

Samples	Space group	a (Å)	c (Å)	V (Å^3)	S_{BET} (m^2/g)
Sr_2TiO_4	$I4/mmm$	3.8858(1)	12.5967(3)	190.204(8)	0.9(1)
$Sr_2TiO_3F_2$	$P4/nmm$	3.7980(2)	15.5517(11)	224.327(32)	1.6(2)
Sr_2TiO_4-N	$I4/mmm$	3.8857(1)	12.5959(3)	190.185(7)	4.8(1)
Sr_2TiO_4-NF	$I4/mmm$	3.8866(1)	12.5988(2)	190.312(3)	4.9(1)

Supplementary Table 2. Comparisons of POWS activity over some reported photocatalysts active to visible light

Photocatalyst	Catalyst dosage (g)	Cocatalyst	Gas evolution rate (μmol/h)	AQE	STH	Ref.
Ta_3N_5	0.3	0.02 wt% Rh/0.06 wt% Cr_2O_3	~6.4 for H_2, ~2.6 for O_2	0.22% (λ = 420 ± 25 nm)	0.014%	[1]
$SrTaO_2N$	0.15	4 wt% CrO_y/4 wt% Ru/1 wt% IrO_2(MW)	-	0.34% (λ = 420 ± 30 nm)	0.0063%	[2]
$BaTaO_2N$	0.2	1 wt% Rh/1 wt% Cr_2O_3/0.3 wt% IrO_2	~0.27 for H_2, ~0.12 for O_2	0.08% (λ = 420 ± 20 nm)	0.0005%	[3]
$LaMg_{1/3}Ta_{2/3}O_2N$	0.2	0.5 wt% $RhCrO_y$	-	0.03% (λ = 440 ± 30 nm)	-	[4]
$Y_2Ti_2O_5S_2$	0.2	1.5 wt% Cr_2O_3/2 wt% Rh/0.3 wt% IrO_2	~4.0 for H_2, ~2.1 for O_2	0.36% (λ = 420 ± 13 nm)	0.007%	[5]
$PbTiO_3$	0.1	0.25 wt% Rh/0.25 wt% Cr_2O_3	~3.29 for H_2, ~1.74 for O_2	0.027% (λ = 420 ± 20 nm)	-	[6]
$BiVO_4$	0.01	2 wt% Rh/2 wt% Cr/0.5 wt% MnO_x	-	0.025% (λ = 420 ± 20 nm)	0.012%	[7]
$NiTi_{0.99}Ga_{0.01}O_3$	0.05	4 wt% Co/1 wt% Pt	-	0.18% (λ = 420 ± 20 nm)	-	[8]
$BaTaO_2N$:Mg	0.05	6 wt% Rh/6 wt% Cr_2O_3/0.3 wt% IrO_2	~0.21 for H_2, ~0.11 for O_2	0.08% (λ = 420 ± 20 nm)	0.0004%	[9]
TaON:Zr	0.15	4 wt% Ru/4 wt% Cr/0.6 wt% IrO_2	~3.0 for H_2, ~1.4 for O_2	0.66% (λ = 420 ± 20 nm)	0.009%	[10]
F/N co-doped Sr_2TiO_4	0.4	0.5 wt% $RhCrO_y$	~12.1 for H_2, ~6.1 for O_2	0.39% (λ = 420 ± 20 nm)	0.028%	This work

Supplementary Figures

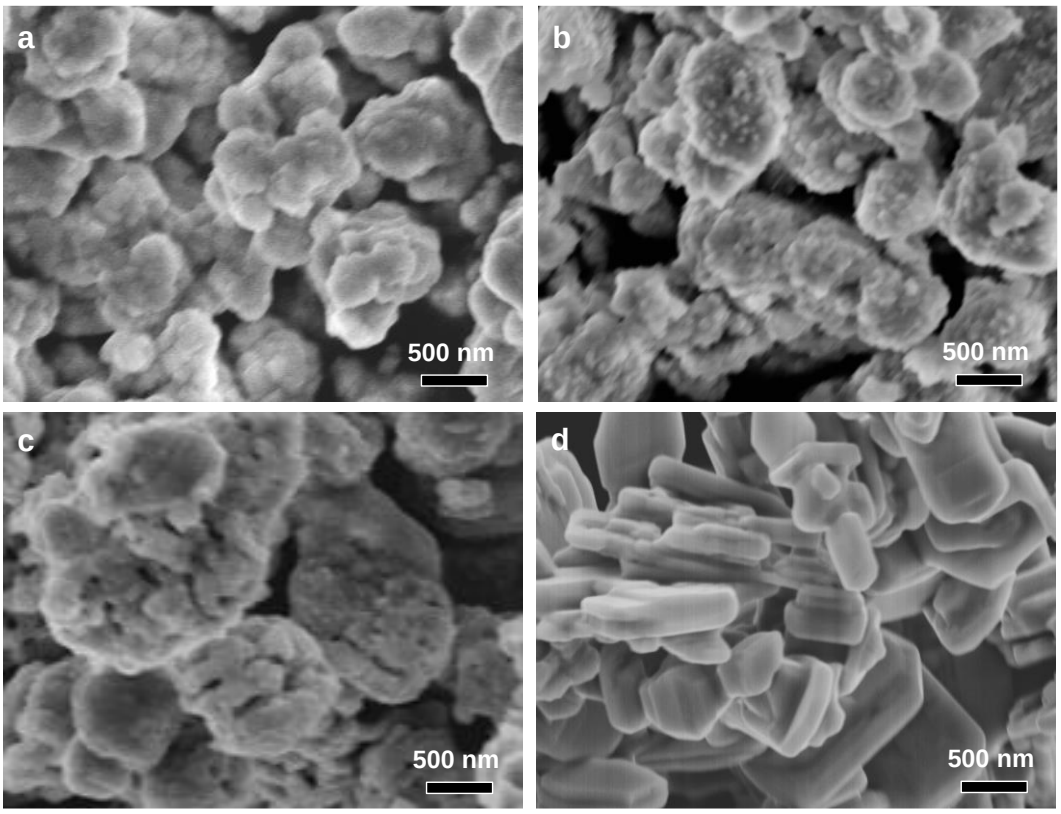

Supplementary Fig. 1 FE-SEM images of the precursor powders: **a** Sr_2TiO_4. **b** $Sr_2TiO_3F_2$. **c** Sr_2TiO_4-N. **d** Sr_2TiO_4-NF.

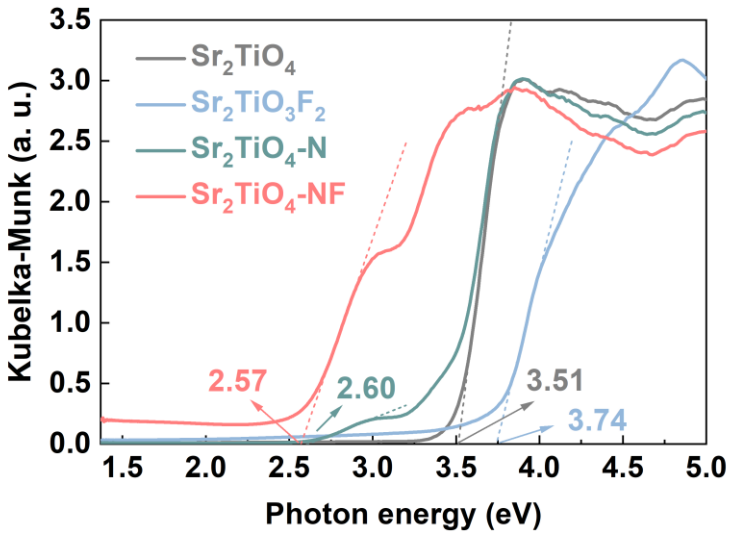

Supplementary Fig. 2 Bandgap determination from UV-Vis DRS spectra of Sr_2TiO_4, $Sr_2TiO_3F_2$, Sr_2TiO_4-N and Sr_2TiO_4-NF

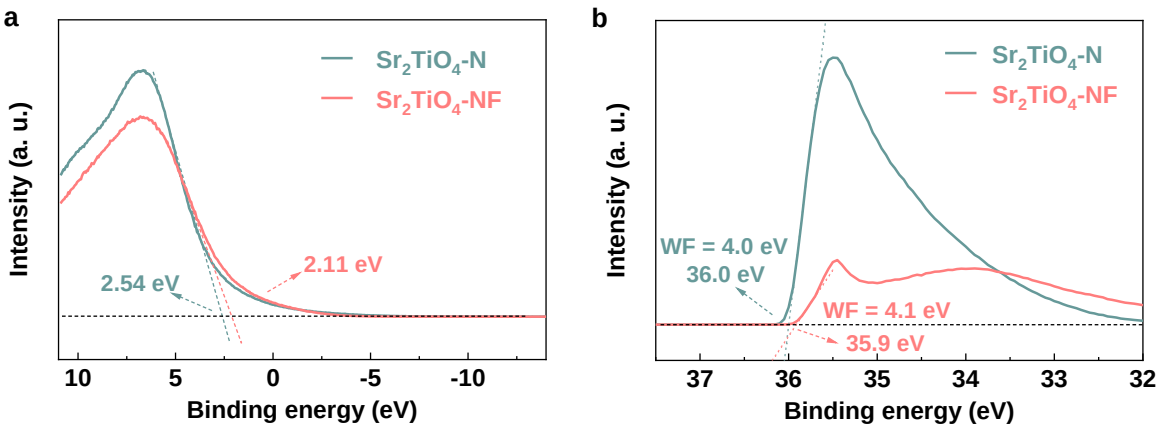

Supplementary Fig. 3 a UPS valence band spectra of Sr_2TiO_4-N and Sr_2TiO_4-NF. **b** UPS secondary electron cutoff spectra of Sr_2TiO_4-N and Sr_2TiO_4-NF, work function (WF) is deduced based on the energy difference between incident photons (40 eV) and the cutoff energy.

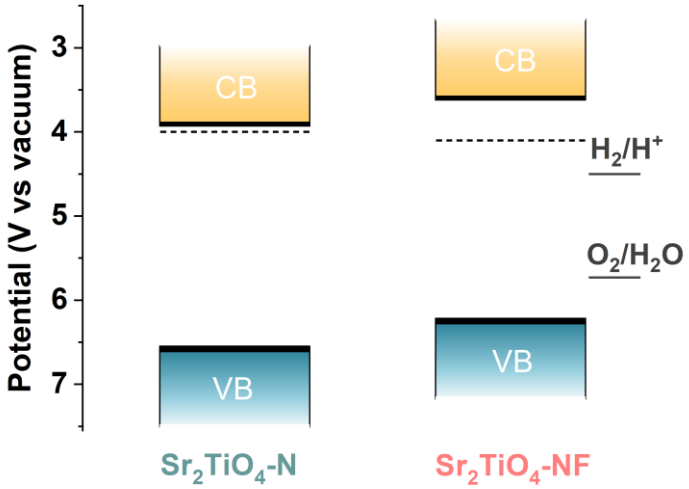

Supplementary Fig. 4 Schematic illustration of UPS-deduced band edge positions of Sr_2TiO_4-N and Sr_2TiO_4-NF, fermi level is denoted by dashed lines and the potential scale is defined by referring to the vacuum level at 0.0 V.

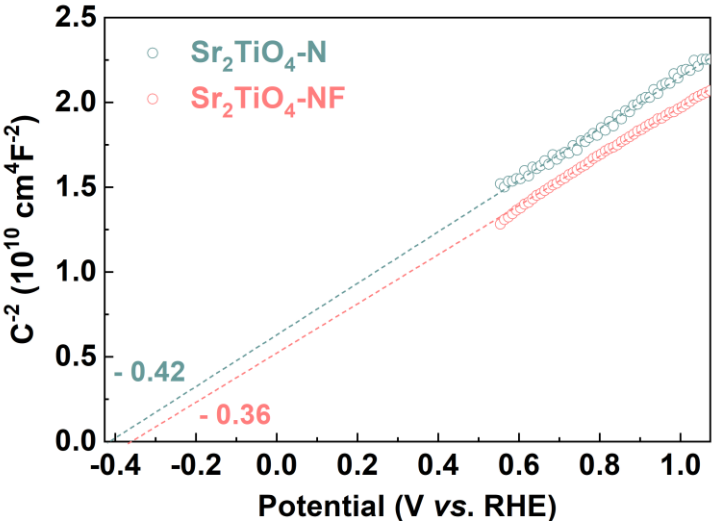

Supplementary Fig. 5 Mott-Schottky (MS) plot of Sr_2TiO_4-N and Sr_2TiO_4-NF, flat-band potential is determined by extrapolating the MS curves down to energy axis.

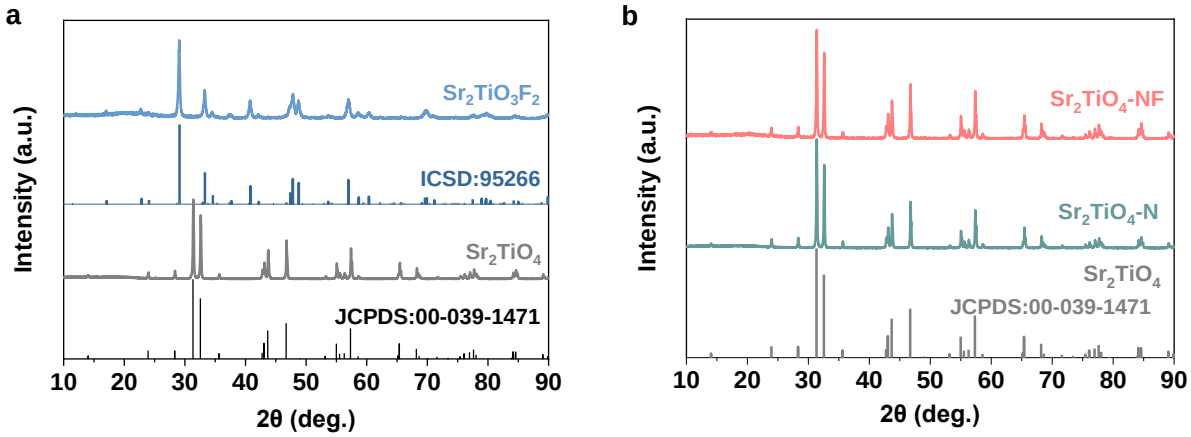

Supplementary Fig. 6 a XRD patterns of $Sr_2TiO_3F_2$ and Sr_2TiO_4 precursors. **b** XRD patterns of Sr_2TiO_4-N and Sr_2TiO_4-NF.

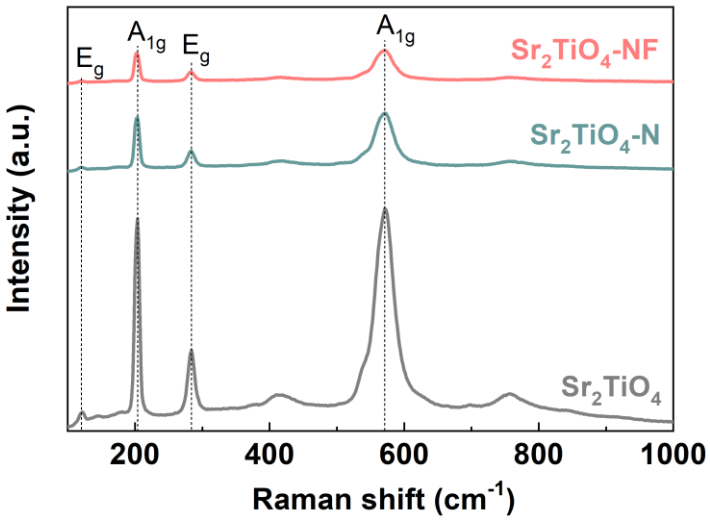

Supplementary Fig.7 Raman spectra of Sr_2TiO_4-NF and Sr_2TiO_4-N, the main Raman active modes (A_{1g} and E_g) for Sr_2TiO_4 are maintained in both samples.

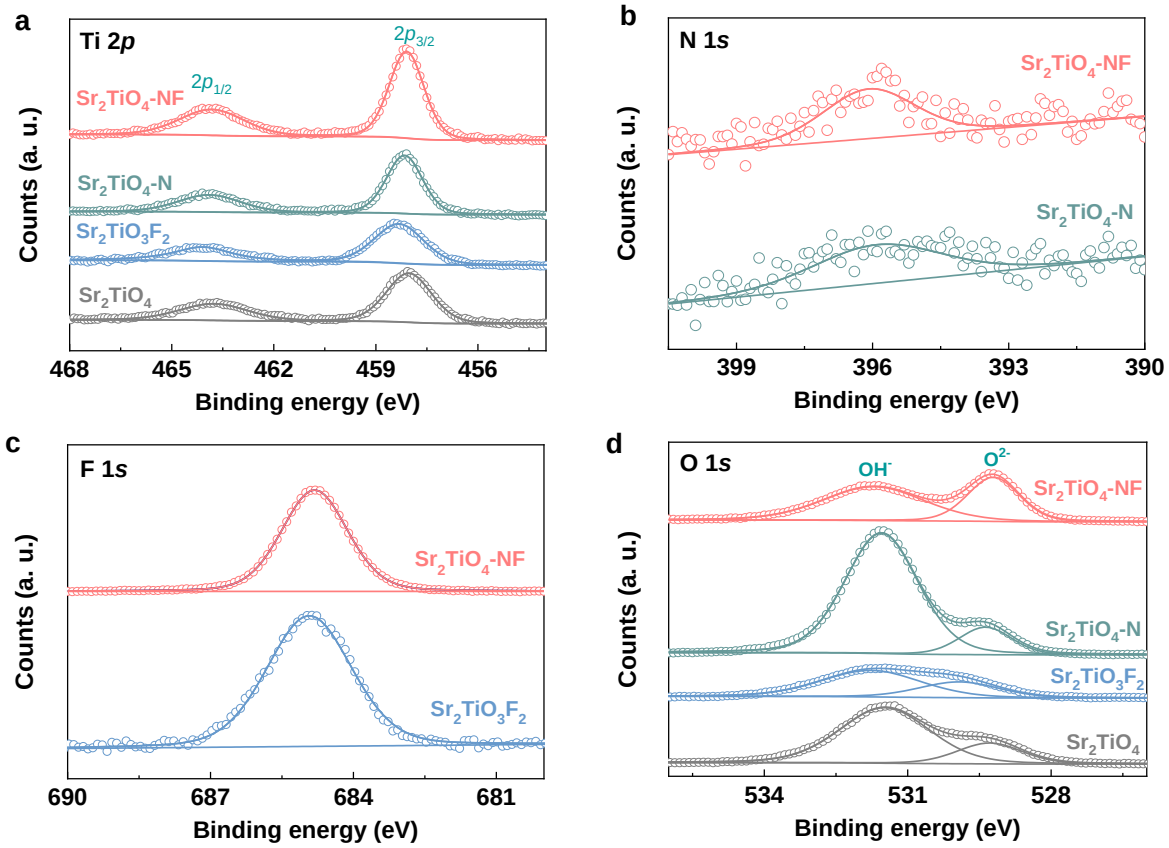

Supplementary Fig. 8 XPS spectra of Sr_2TiO_4, $Sr_2TiO_3F_2$, Sr_2TiO_4-N and Sr_2TiO_4-NF: **a** Ti 2*p*, **b** N 1*s*, **c** F 1*s*, **d** O 1*s*.

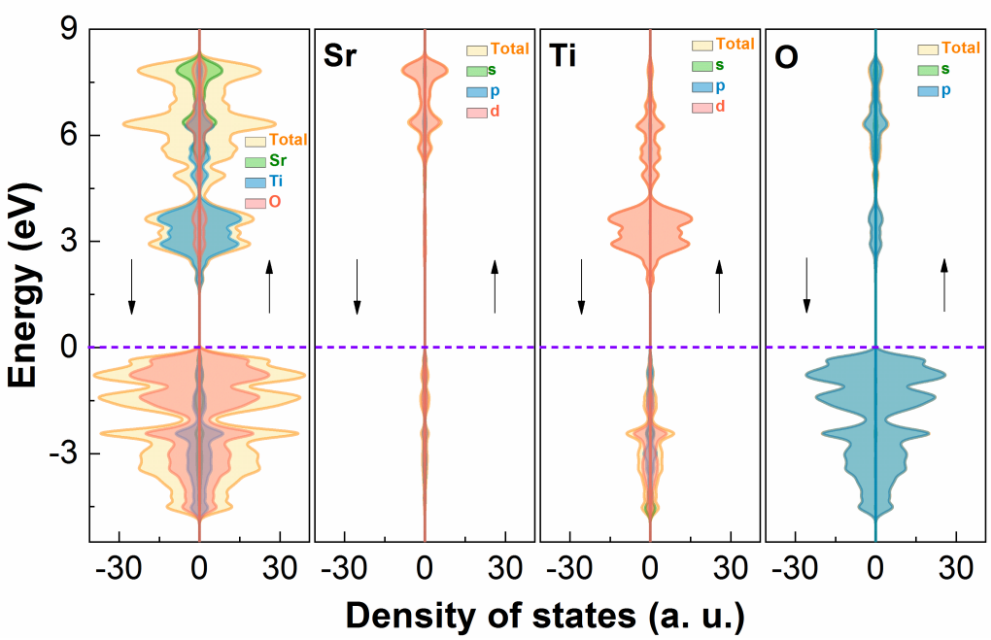

Supplementary Fig.9 Band structure, density of states (DOS) and projected density of states (PDOS) of Sr_2TiO_4, Fermi level is denoted by the dashed purple lines.

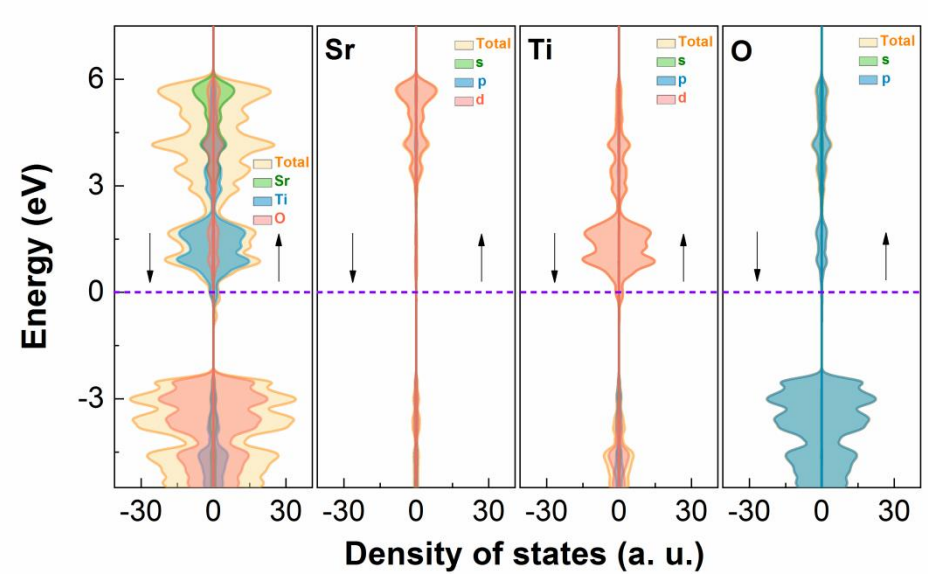

Supplementary Fig. 10 Band structure, density of states (DOS) and projected density of states (PDOS) of Sr_2TiO_4 containing Ti^{3+} and V_O defects, Fermi level is denoted by the dashed purple lines.

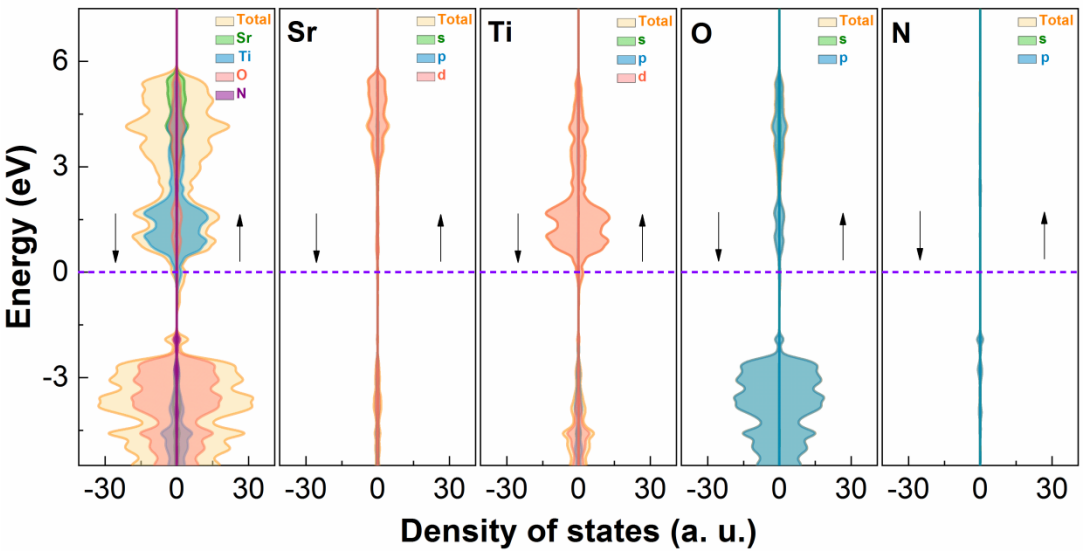

Supplementary Fig. 11 Band structure, density of states (DOS) and projected density of states (PDOS) of Sr_2TiO_4 containing Ti^{3+}, V_O and N_O defects, Fermi level is denoted by the dashed purple lines.

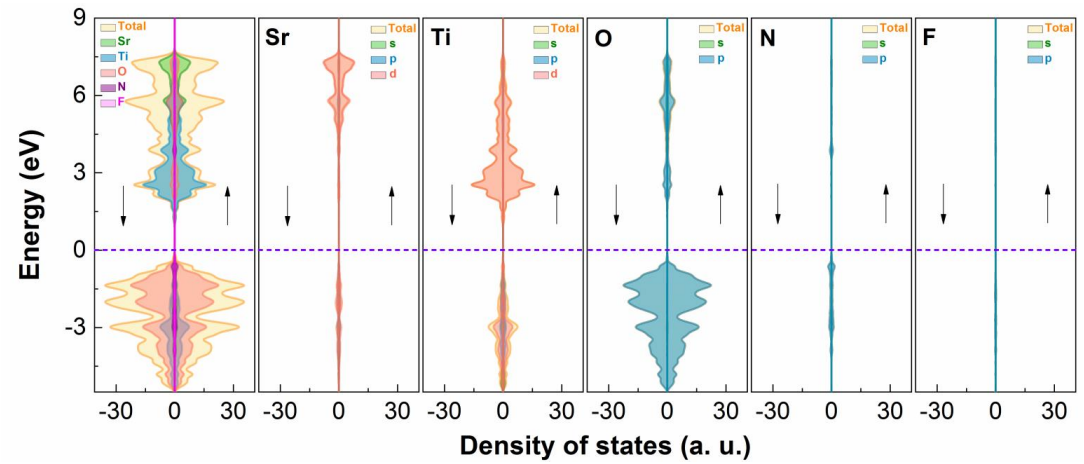

Supplementary Fig. 12 Band structure, density of states (DOS) and projected density of states (PDOS) of Sr_2TiO_4 containing F_O and N_O defects, Fermi level is denoted by the dashed purple lines.

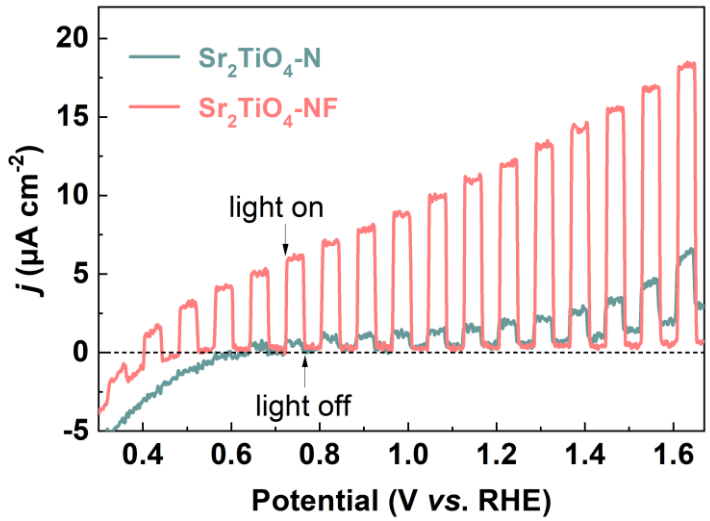

Supplementary Fig. 13 Linear scan voltammetry (LSV) curves of photoelectrodes fabricated by Sr_2TiO_4-N and Sr_2TiO_4-NF powders under chopped visible light illumination ($\lambda \geq 420$ nm). The potential is not iR corrected. The area of the photoelectrode is 1 cm^2.

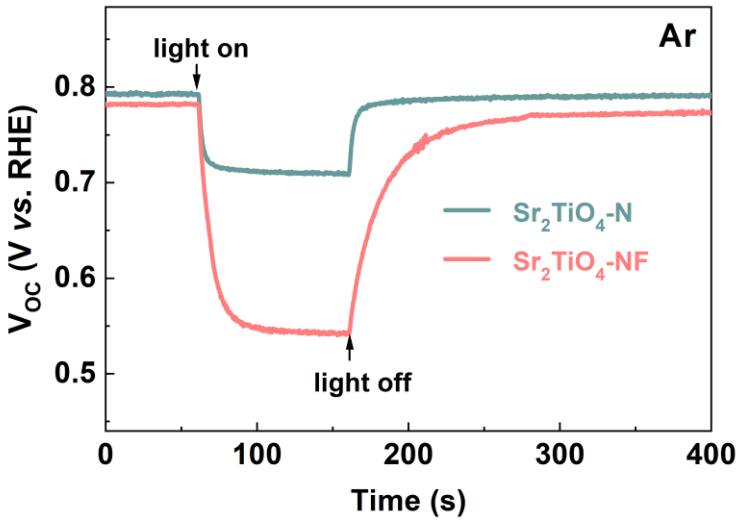

Supplementary Fig. 14 Open-circuit voltage (V_{OC}) decay profiles of Sr_2TiO_4-N and Sr_2TiO_4-NF in Ar. The potential is not iR corrected.

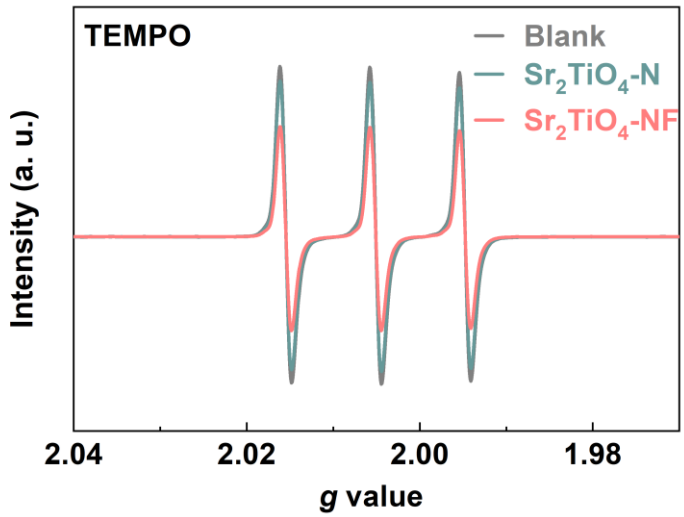

Supplementary Fig. 15 EPR spectra of TEMPO in the presence and absence of light-illuminated Sr_2TiO_4-N and Sr_2TiO_4-NF for 8 s

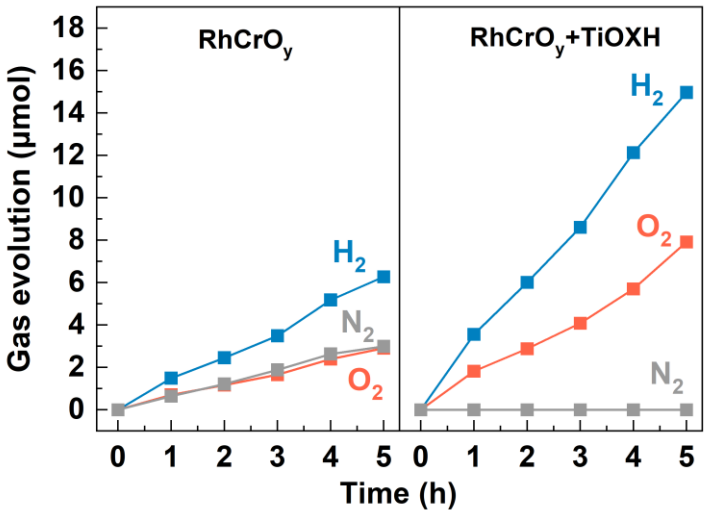

Supplementary Fig. 16 Temporal gas evolution (H_2, O_2 and N_2) over Sr_2TiO_4-NF coated with or without TiOXH (1 wt%) under visible light illumination ($\lambda \geq 420$ nm). $RhCrO_y$ (0.5 wt%) was loaded as a cocatalyst.

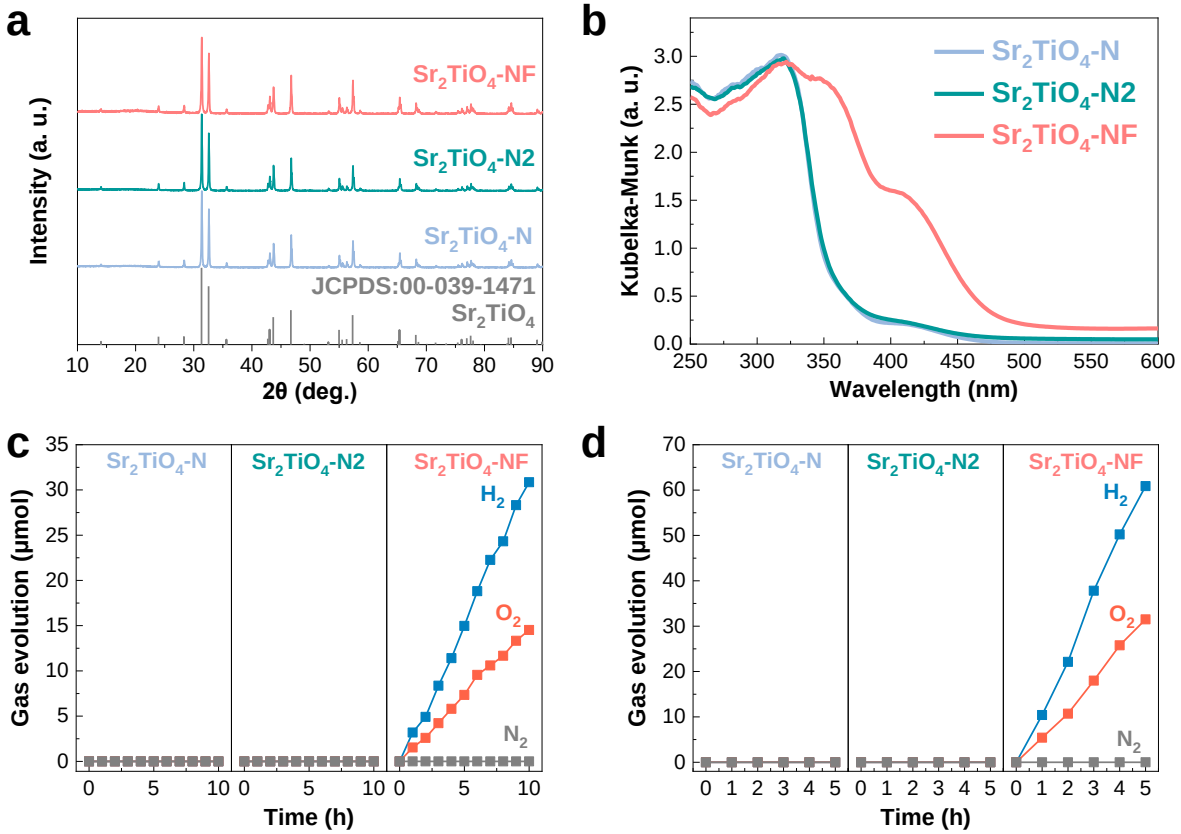

Supplementary Fig. 17 a XRD patterns of Sr_2TiO_4-N, Sr_2TiO_4-N2, and Sr_2TiO_4-NF, standard patterns of Sr_2TiO_4 are also included for comparisons; **b** UV-vis DRS spectra of Sr_2TiO_4-N, Sr_2TiO_4-N2, and Sr_2TiO_4-NF; **c** photocatalytic overall water splitting for Sr_2TiO_4-N, Sr_2TiO_4-N2, and Sr_2TiO_4-NF under visible light ($\lambda \geq 420$ nm); **d** photocatalytic overall water splitting for Sr_2TiO_4-N, Sr_2TiO_4-N2, and Sr_2TiO_4-NF under simulated sunlight (100 $mW \cdot cm^{-2}$). Reaction conditions: 0.4 g catalysts, $RhCrO_y$ (0.5 wt%) cocatalyst, 100 mL deionized water.

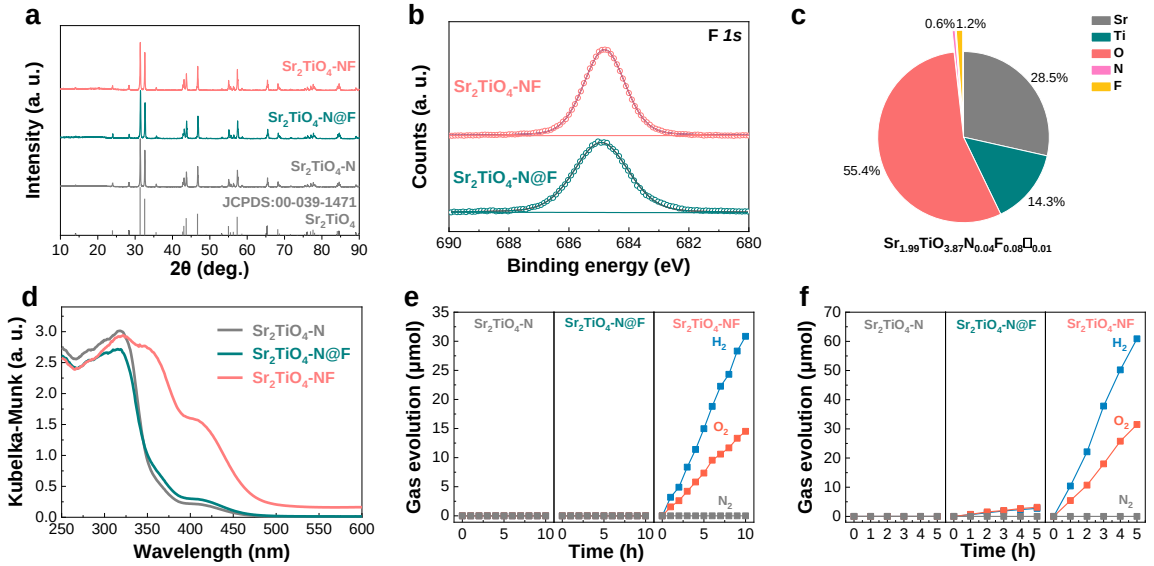

Supplementary Fig. 18 **a** XRD patterns of Sr_2TiO_4-N, Sr_2TiO_4-N@F, and Sr_2TiO_4-NF, standard patterns of Sr_2TiO_4 are also included for comparisons; **b** XPS F 1*s* spectra of Sr_2TiO_4-N@F and Sr_2TiO_4-NF; **c** element content of Sr_2TiO_4-N@F by ICP, ONH and ion chromatograph analysis, deduced chemical formula are shown at the bottom (oxygen vacancies are represented by empty squares '□'); **d** UV-vis DRS spectra of Sr_2TiO_4-N, Sr_2TiO_4-N@F, and Sr_2TiO_4-NF; **e** photocatalytic overall water splitting for Sr_2TiO_4-N, Sr_2TiO_4-N@F, and Sr_2TiO_4-NF under visible light ($\lambda \geq 420$ nm); **f** photocatalytic overall water splitting for Sr_2TiO_4-N, Sr_2TiO_4-N@F, and Sr_2TiO_4-NF under simulated sunlight (100 $mW \cdot cm^{-2}$). Reaction conditions: 0.4 g catalysts, $RhCrO_y$ (0.5 wt%) cocatalyst, 100 mL deionized water.

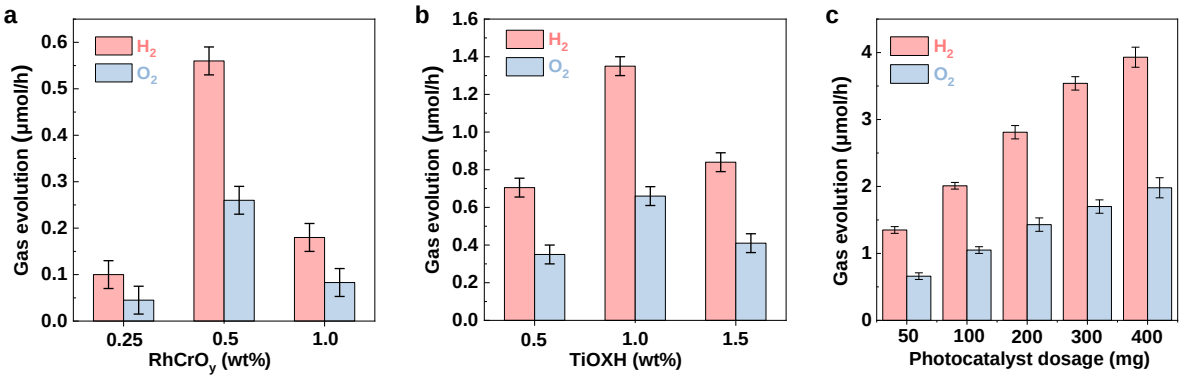

Supplementary Fig. 19 POWS activity over Sr_2TiO_4-NF as a function of: **a** $RhCrO_y$ content, TiOXH content is fixed at 1 wt%, catalyst dosage is fixed at 50 mg; **b** TiOXH content, $RhCrO_y$ content is fixed at 0.5 wt%, catalyst dosage is fixed at 50 mg; **c** catalyst dosage, $RhCrO_y$ content is fixed at 0.5 wt%, TiOXH content is fixed at 1 wt%. The error bars correspond to the standard deviations of the measurements repeated for three times.

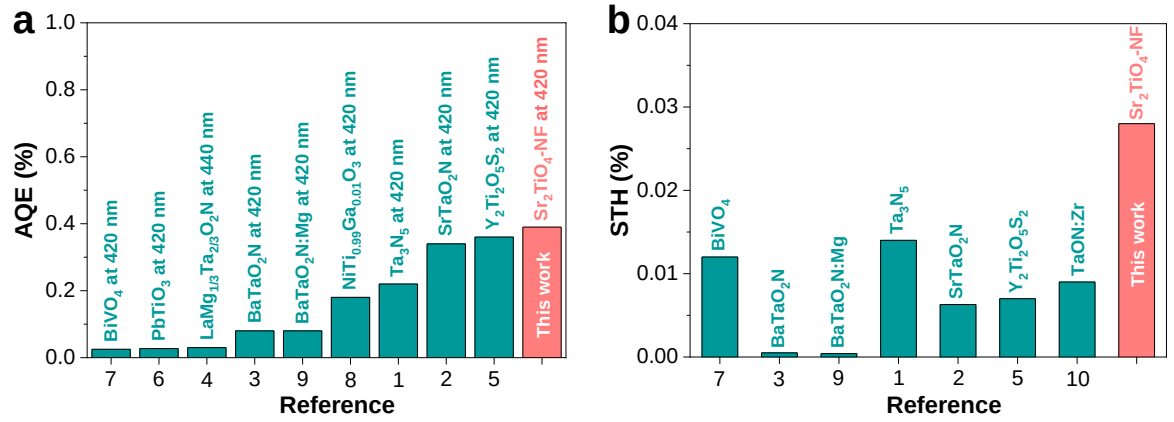

Supplementary Fig. 20 (a) Comparisons of visible-light-active compounds reported for POWS: (a) AQE of POWS under visible light; (b) STH of POWS. More detailed information can be found in **Supplementary Table 2**.

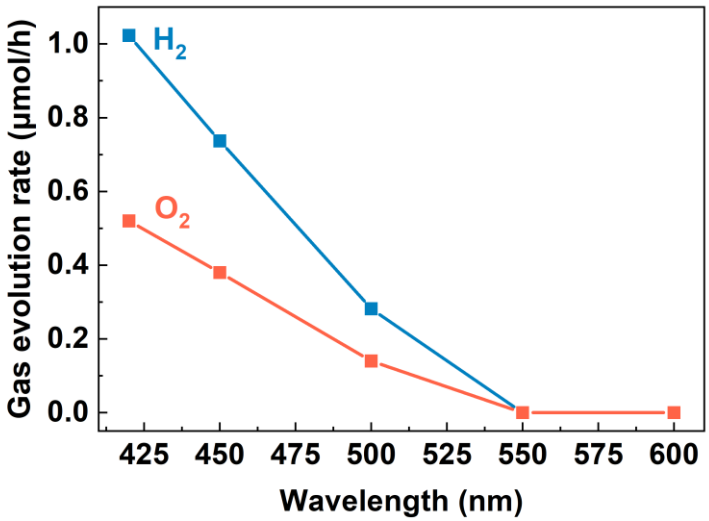

Supplementary Fig. 21 Gas evolution rate as a function of wavelength over Sr_2TiO_4-NF.

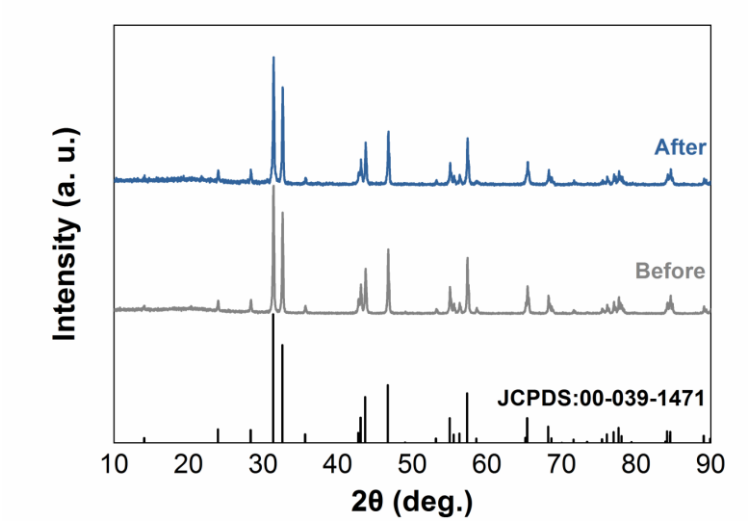

Supplementary Fig. 22 XRD patterns of Sr_2TiO_4-NF before and after photocatalytic overall water splitting reactions, standard patterns of Sr_2TiO_4 are also included for comparisons.

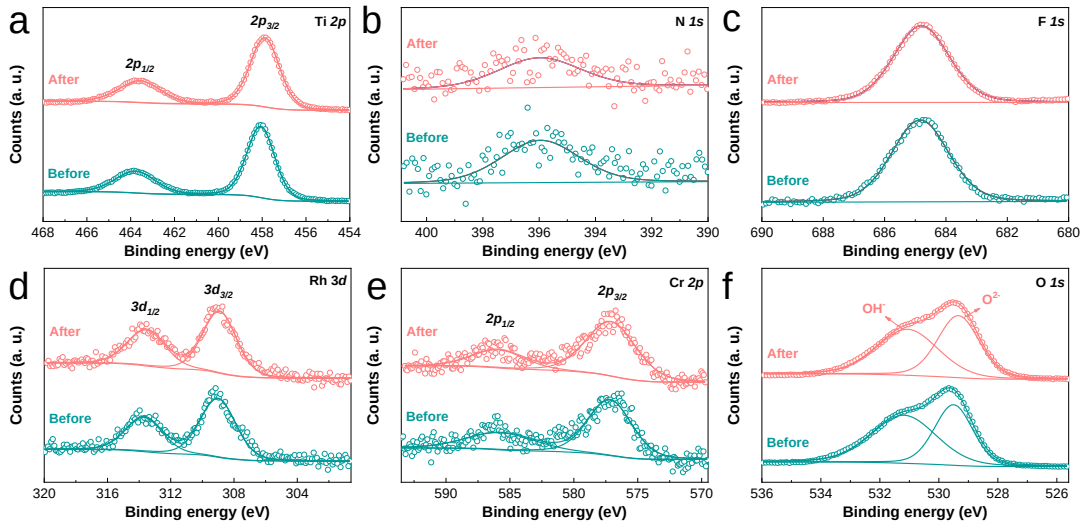

Supplementary Fig. 23 XPS of Sr_2TiO_4-NF before and after photocatalytic overall water splitting reactions: **a** Ti 2*p*; **b** N 1*s*; **c** F 1*s*; **d** Rh 3*d*; **e** Cr 2*p*; **f** O 1*s*.

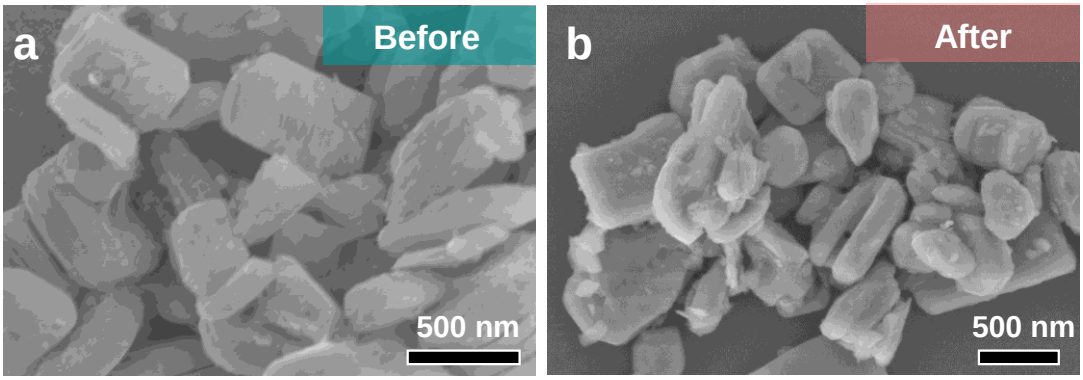

Supplementary Fig. 24 SEM image of Sr_2TiO_4-NF before and after photocatalytic overall water splitting reactions: **a** before; **b** after.

Supplementary References

1. Wang Z., *et al.* Overall water splitting by Ta_3N_5 nanorod single crystals grown on the edges of $KTaO_3$ particles. *Nat. Catal.* **1**, 756-763 (2018).
2. Chen K. H., *et al.* Overall Water Splitting by a $SrTaO_2N$-Based Photocatalyst Decorated with an Ir-Promoted Ru-Based Cocatalyst. *J. Am. Chem. Soc.* **145**, 3839-3843 (2023).
3. Nishimae S., *et al.* Active BaTaO2N photocatalysts prepared from an amorphous Ta_2O_5 precursor for overall water splitting under visible light. *J. Mater. Chem. A* **11**, 6299-6310 (2023).
4. Pan C. S., *et al.* A Complex Perovskite-Type Oxynitride: The First Photocatalyst for Water Splitting

Operable at up to 600 nm. *Angew. Chem. Int. Ed.* **54**, 2955-2959 (2015).

5. Wang Q.*, et al.* Oxysulfide photocatalyst for visible-light-driven overall water splitting. *Nat. Mater.* **18**, 827-832 (2019).
6. Wan G. D.*, et al.* Photocatalytic Overall Water Splitting over $PbTiO_3$ Modulated by Oxygen Vacancy and Ferroelectric Polarization. *J. Am. Chem. Soc.* **144**, 20342-20350 (2022).
7. Dai D. J.*, et al.* Strain Adjustment Realizes the Photocatalytic Overall Water Splitting on Tetragonal Zircon $BiVO_4$. *Adv. Sci.* **9**, 2105299 (2022).
8. Wang L., Kong Y. H., Fang Y. X., Cai P. R., Lin W., Wang X. C. A Ga Doped $NiTiO_3$ Photocatalyst for Overall Water Splitting under Visible Light Illumination. *Adv. Funct. Mater.* **32**, 2208101 (2022).
9. Li H. H.*, et al.* One-Step Excitation Overall Water Splitting over a Modified Mg-Doped $BaTaO_2N$ Photocatalyst. *ACS Catal.* **12**, 10179-10185 (2022).
10. Xiao J. D.*, et al.* Enhanced Overall Water Splitting by a Zirconium-Doped TaON-Based Photocatalyst. *Angew. Chem. Int. Ed.* **61**, e202116573 (2022).